Light charged particle and intermediate mass fragment emission in the reaction 640 MeV ^{86}Kr + ^{63}Cu

J. Boger,* John M. Alexander, G. Auger,† A. Elmaani,‡ S. Kox,§ Roy A. Lacey, and A. Narayanan ‖
Department of Chemistry, State University of New York at Stony Brook, Stony Brook, New York 11794

Morton Kaplan and D. J. Moses
Department of Chemistry, Carnegie Mellon University, Pittsburgh, Pennsylvania 15213

M. A. McMahan
Lawrence Berkeley Laboratory, Berkeley, California 94720

P. A. DeYoung and C. J. Gelderloos¶
Department of Physics, Hope College, Holland, Michigan 49423

G. Gilfoyle
Department of Physics, University of Richmond, Richmond, Virginia 23173
(Received 28 April 1993)

Light-charged particles from the reaction 640 MeV ^{86}Kr + ^{63}Cu have been measured in singles and in coincidence with intermediate mass fragments, fissionlike fragments, and other light-charged particles. Multiplicities for ^{1}H and ^{4}He in association with the evaporation residues, fragments, and intermediate mass fragments have been determined. Composite nuclei, most of which decay to evaporation residues, are the major sources of evaporative light-charged particle emission. Average multiplicities for prescission ^{1}H and ^{4}He can be associated with the composite nucleus *en route* to scission; they are relatively large and thus suggest a time scale for fission longer than that for evaporation. The multiplicities for ^{1}H and ^{4}He in association with the intermediate mass fragments indicate that these fragments are usually born with a significant quantity of excitation energy. These multiplicities are used to estimate the primary masses and kinetic energies of the intermediate mass fragments.

PACS number(s): 24.60.Dr, 25.70.Gh, 25.70.Jj

I. INTRODUCTION

One of the major goals in studies of heavy-ion reactions is to understand the statistical properties of hot rotating nuclei. Statistical-model reaction simulations are routinely used in conjunction with experimental data in order to infer these properties. In particular, coincidence measurements between light-charged particles and fragments have played an important role in exploring average emitter shapes, temperatures, spins, and multiplicities for ^{1}H and ^{4}He in association with various emission sources such as the fragments and the prescission nucleus (see, for example, [1]).

In this work, we study the reaction 640 MeV ^{86}Kr + ^{63}Cu, chosen to match earlier studies of 337 MeV ^{40}Ar + ^{nat}Ag [1,2]. Both reactions are expected to produce the same composite nucleus, ^{149}Tb*, with an excitation energy of 194 MeV. In the accompanying paper [3], we compare the results of these two works in order to test for and identify equilibrium properties of the intermediate nuclei. In this report, the goal is to identify the mechanistic origins of the light-charged particles produced in the ^{86}Kr reaction and to characterize the properties of their emitters. In addition, multiplicities are reported for ^{1}H and ^{4}He in association with the intermediate mass fragments (IMF).

Experimental aspects are given in Sec. II, then we examine various inclusive ^{1,2,3}H and ^{4}He measurements in Sec. III. We find that the dominant mechanism of the light-charged particle (LCP) production is evaporation. Next, we present in Sec. IV fragment-particle coincidence data, which are interpreted via the statistical-model code GANES [4]. In Secs. V and VI, we explore the mechanistic implications of the fragment-particle coinci-

*Texas A&M University, Cyclotron Institute, College Station, TX 77843-3366.
†Grand Accelerateur National d'Ions Lourds, B. P. 5027, Caen 14021, France.
‡University of Washington, Nuclear Physics Lab. GL-10, Seattle, WA 98195.
§Institut des Sciences Nucléaires de Grenoble, F38026, Grenoble CEDEX, France.
‖Department of Chemistry, Brock University, St. Catharines, Ontario, Canada L2S3A1.
¶Department of Physics, State University of New York at Stony Brook, Stony Brook, NY 11794.

dence measurements and find that most of the inclusive and particle-particle coincidence production of LCP's is associated with evaporation and often the evaporation residues. We also find that the prescission light-charged particle multiplicities are quite significant, suggesting a relatively slow fission process during which particle evaporation may occur. Similar observations have been made before for 337 MeV ^{40}Ar + ^{nat}Ag [1].

Inclusive IMF's and their light-charged particle multiplicities were also studied for this reaction. Previous work [5] has shown for the reaction 640 MeV ^{86}Kr + ^{63}Cu that binary fission-like breakup is the dominant mechanism for IMF production. In Sec. VII these multiplicities are used to derive the primary masses of the IMFs and the total kinetic energy released in these very asymmetric binary breakups. An appendix is provided that details how these masses and energies were derived.

II. EXPERIMENTAL

Two experiments were performed using beams of 640 MeV ^{86}Kr provided by the Lawrence Berkeley Laboratory SuperHILAC. Copper target thicknesses were 897 μg/cm^2 and 1030 μg/cm^2, as determined by Rutherford scattering in comparison to a ^{197}Au target of known thickness.

In the first experiment, two GASP (gas and silicon and plastic) detectors were positioned in the horizontal plane for the detection of the fragments such that each detector was centered at 35° to the beam in the standard configuration: one GASP to the left of the beam, one to the right. Solid angles were $\approx$ 6 msr. The gas pressure was 50 torr of isobutane for the ΔE signal, and each GASP had a Si stopping detector of $\approx$ 1000 microns thick. Light-charged particles were measured in singles and in coincidence with fragments using four solid-state telescopes (SST), each composed of three elements. Two of these SST's were placed at +50° and −50° to the beam. These SST's detected light-charged particles in the plane defined by the beam and a fragment detected by either of the GASP's. The other two SST's were placed at +5° and +55° directly above the beam, providing for out-of-plane light-charged particle coincidence measurements. Particle-particle coincidence measurements were also made between pairs of SST's. Solid angles of the SST's ranged from 1.5 to 10 msr.

The second experiment was similar to the first. In place of GASPS's, two "wedge" detectors [6] were used for the detection of both ^{4}He particles and the heavier fragments. They were placed on either side of the beam. These detectors are composed of 5 coplanar solid-state stopping detectors spaced at 10° intervals with a common gas ionization chamber to provide a ΔE signal. Alpha particles and fragments were measured in singles or in coincidence with fragments that registered in any of three gas ionization chambers (GT's). These GT's were also equipped with solid-state stopping detectors and were placed, one each, at 18° above and below the beam and one at −18° to the beam in the same plane as the wedge detectors. Average beam currents for both experiments ranged from approximately 5 nA for inclusive measurements up to 30 nA for the coincidences.

III. INCLUSIVE LIGHT-CHARGED PARTICLE MEASUREMENTS

We begin by examining inclusive measurements of the light-charged particles. These particles are produced by a variety of sources and over a broad time range from very fast prethermalization emission to the slower evaporative processes. Despite the possible complexity of these emissions, we are nevertheless able to identify the dominant processes involved in their production. For the reaction studied here, we find that the predominant mechanism for the production of light-charged particles is evaporation.

This is illustrated in Fig. 1, which is a velocity contour map of the invariant cross section for inclusive ^{4}He production. This contour map has been plotted as a function of the velocity components parallel ($v_\parallel$) and perpendicular ($v_\perp$) to the beam. Our forward-angle detectors provide a good overview of the evaporative component of the reaction due to the use of reversed kinematics [7]. The detectors were placed in the backward direction with respect to the direction of the light reaction partner (i.e., in the forward hemisphere in the laboratory). Concentric circles in Fig. 1 are drawn with their centers on the tip of the $v_{c.m.}$ vector, which represents the recoil velocity for complete fusion of target and projectile. Figure 1 illustrates that, even for inclusive measurements, the predominant source of ^{4}He emission is essentially isotropic emission from a source moving with its average velocity equal to that of the center of mass. Preequilibrium processes would lead to strong deviations from these velocity circles, especially for the more energetic particles, if this were a major component of the inclusive ^{4}He cross section. We therefore identify evaporation as the major

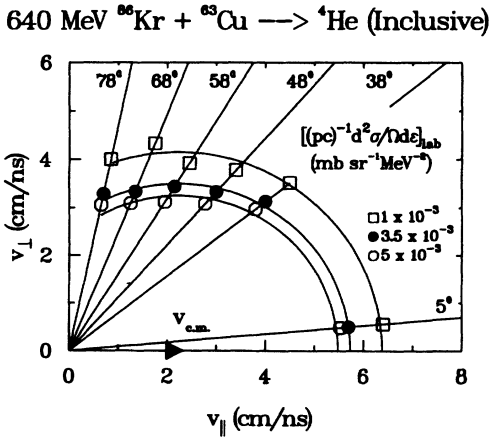

FIG. 1. Contour map of the invariant cross section for inclusive ^{4}He emission from the reaction ^{86}Kr + ^{63}Cu. The contours are plotted as a function of velocity perpendicular ($v_\perp$) and parallel ($v_\parallel$) to the beam. The velocity, $v_{c.m.}$, is for a recoiling nucleus produced by complete fusion of target and projectile.

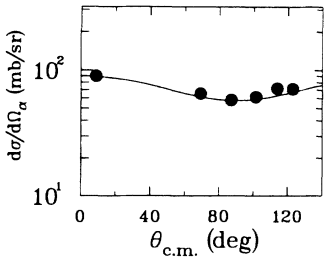

FIG. 2. Angular distribution in the c.m. for inclusive ^{4}He emission. The line through the experimental points is to guide the eye.

mechanism for the production of these particles. (There may, of course, be preequilibrium emission in the backward hemisphere that is out of sight in Fig. 1).

The evaporative nature of the ^{4}He particle is also illustrated in the inclusive angular distribution shown in Fig. 2. The symmetry about 90° and the near isotropy of the angular distribution show that in the center-of-mass (c.m.) frame, the emitters have only a weak memory of the beam direction. This picture is consistent with evaporative emission from a long-lived, rotating composite nucleus so that its spin axis is the only cause for remembrance of the two-body entrance channel directions of target and projectile.

Finally, in Fig. 3, we present typical energy spectra for ^{1,2,3}H and ^{4}He for the c.m. angles indicated. These are channel energy spectra and have been transformed into the c.m. on an event-by-event basis. Their Maxwellian shapes and low apparent temperatures (or steep high energy slopes) are almost independent of angle. This gives indications that these spectra are derived from evaporative mechanisms.

The combined observations of the ^{4}He invariant cross section, inclusive ^{4}He angular distribution, and ^{1,2,3}H and ^{4}He energy spectra lead one to the conclusion that these particles are predominantly evaporative in origin. Angle-integrated inclusive (singles) ^{1}H and ^{4}He cross sections are summarized in Table I; they were obtained with the assumption of symmetry about 90° in the c.m. (i.e., only the evaporative component).

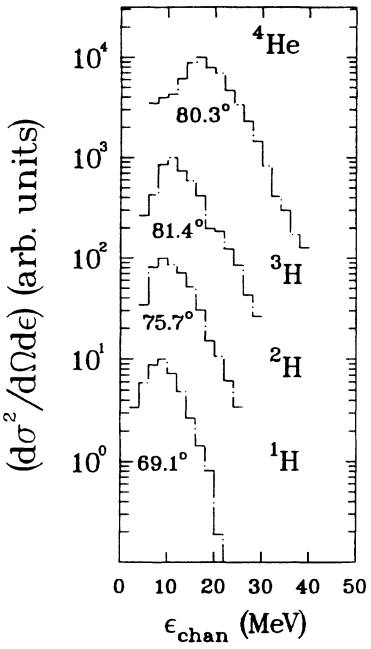

FIG. 3. Inclusive ^{1,2,3}H and ^{4}He channel energy spectra for the indicated c.m. angles.

IV. INCLUSIVE FRAGMENT AND FRAGMENT-PARTICLE COINCIDENCE MEASUREMENTS

A. Inclusive fusion-fission and deeply inelastic reactions

Inclusive fragments of $12 \leq Z \leq 55$ were detected at a laboratory angle of 18° (second experiment). The resulting differential cross section was then transformed to the c.m., based on a single Jacobian value calculated for the velocity of the average fragment [8]. In a related study of the reaction ^{40}Ar + ^{nat}Ag [1,2], Z's of $24 \leq Z \leq 40$ were selected to obtain the fusion-fission (FF) cross section. For the deeply inelastic cross sections (DIR), two Z ranges were employed: (1) $12 \leq Z_{PLF} \leq 24$ (projectile like fragment) and (2) $40 \leq Z_{TLF} \leq 55$ (targetlike

TABLE I. Fragment and particle cross sections for the reaction 640 MeV ^{86}Kr + ^{63}Cu.

σ(ER) = 360 ±66 mb [a]		σ(FF/DIR) = 550 ±43 mb	
Total ^{1}H and ^{4}He cross sections			
Singles		Double coincidences	
σ_s^p	1106 ±41 mb	σ_{dc}^{pp}	1220 ±150 mb
σ_s^α	875 ±87 mb	$\sigma_{dc}^{\alpha\alpha}$	574 ±68 mb
		$\sigma_{dc}^{p\alpha}$	801 ±140 mb
ER ^{1}H and ^{4}He cross sections			
Singles		Double coincidences	
σ_s^p(ER)	587 ±93 mb	σ_{dc}^{pp}(ER)	894 ±151 mb
σ_s^α(ER)	582 ±49 mb	$\sigma_{dc}^{\alpha\alpha}$(ER)	479 ±68 mb
		$\sigma_{dc}^{p\alpha}$(ER)	520 ±160 mb

[a]Extrapolated from Refs. [17] and [18].

fragment). For such a mass-symmetric entrance channel as ^{86}Kr + ^{63}Cu, it is kinematically difficult to separate DIR from FF processes. The two reactions were therefore treated as one (hereafter referred to as the FF/DIR reaction class) with a combined Z range of $12 \leq Z \leq 55$. The value for the FF/DIR cross section is listed in Table I; it was obtained by assuming a $1/\sin\theta_{\text{c.m.}}$ angular distribution.

B. Fragment-particle coincidence measurements

In order to unravel complexities in light-charged particle emission, we must identify emission sources. Light-charged particles produced in binary fission events may be emitted by any of three sources. These are (1) the composite nucleus prior to fission, (2) the detected trigger fragment, and (3) the undetected fragment. A particle multiplicity may be defined for each of these sources such that, in general, the working equation for this particle multiplicity (for example, protons) triggered by fragments of type X is as follows:

$$\langle m^p(X)\rangle = \frac{\{\int(\frac{d^2\sigma}{d\Omega_{\text{sw}}d\Omega_{\text{tr}}})d\Omega_{\text{sw}}\}^p}{\{(\frac{d\sigma}{d\Omega_{\text{tr}}})\}^X_s} = \frac{\sigma^p(X)}{\sigma_s(X)}, \quad (4.1)$$

where $\langle m^p(X)\rangle$ is the average multiplicity for particle x (e.g., p for proton) and $d\Omega_{\text{tr(sw)}}$ is the differential solid angle for the trigger (sweeper) detector. The numerator represents the differential (or integral) cross section for the particle in coincidence with X. The integral is made over the solid angle of the sweeper detector. The denominator is the singles differential (or integral) cross section for X. We assume that $\langle m^p(X)\rangle$ is independent of the fragment trigger angle. The integrated form in Eq. (4.1) is simply the ratio of the angle-integrated cross sections and may be used when the cross section of the particle is known for source X.

C. Technique for separation of energy spectra into contributions from composite nucleus emission (CE) and fragment emission (FE)

To obtain fragment-particle multiplicities for the ^{149}Tb* composite system, one needs to sort out the various sources of light-charged particle emission. This can be done from the shapes of the laboratory energy spectra, which are comprised of emissions from various sources [9–11]. As this separation cannot be made directly, one must rely on the kinematic shifts of the energy spectra with angle; hence one makes use of a largely kinematic reaction model to simulate the spectral shapes of the various source emissions. The statistical-model code employed in this analysis is known as GANES [4].

The upper right-hand frame of Fig. 4 shows an in-plane vector diagram for the reaction 640 MeV ^{86}Kr + ^{63}Cu that leads to fission and ^{4}He emission. Figure 5 has the same format but for ^{1}H emission. The solid, dashed, and dot-dashed lines represent average velocities of ^{4}He particles emitted isotropically from three sources. The solid

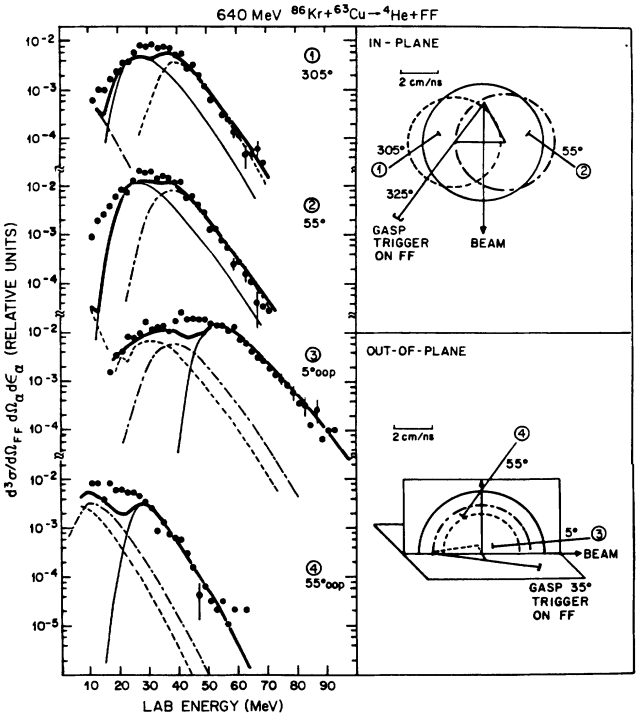

FIG. 4. Fragment-particle coincidence spectra for ^{4}He particles detected in plane (detectors 1 and 2) and out of plane (detectors 3 and 4) with respect to the trigger fragment ($24 \leq Z \leq 40$) at $\theta_{\text{lab}} = 35°$. The points are the experimental data, and the curves are the statistical model simulations of these spectra. The dashed curve represents particle emission from the trigger fragment, the dashed-dot curve from the undetected fragment, and the thin solid line from the composite system prior to fission. The sum of these three contributions is indicated by the thick solid line.

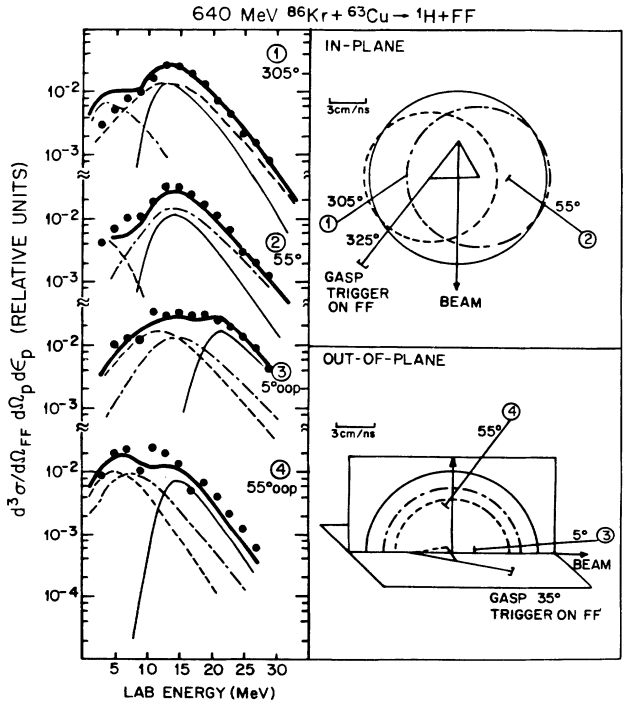

FIG. 5. Same as Fig. 4 but for ^{1}H emission.

circle is centered on the center-of-mass velocity and represents prescission emission from the composite nucleus. The dashed circle (for emission from the detected fragment) is centered on the average velocity of the detected fragment whose lab direction is such that the fragment "strikes" the trigger detector (labeled "GASP") at 325°. Finally, the dot-dashed circle (for emission from the undetected fragment) is centered on the average velocity of the undetected fragment. Four SST's are positioned at four angles: 55° (to the left) and 305° (to the right) of the beam, respectively, and 5° and 55° directly above the beam (seen in the out-of-plane diagram). The corresponding ^{4}He lab energy spectra for each SST are shown on the left side of the figure. By triggering on a fragment, we look only at decay chains that lead to fission. This excludes any ER component from these energy spectra. The light solid, dashed, and dot-dashed smooth curves on the left represent simulated energy spectra for ^{4}He emission from each source. The same line types are used in these energy spectra as in the vector diagrams.

Turn again to the in-plane vector diagram, specifically at SST 1. It will be noted that as it lies on the same side of the beam as the trigger, it will preferentially receive emission from the trigger fragment. Furthermore, ^{4}He emitted from the trigger fragment will, on average, have higher velocities, hence energies, than those from the other sources, as seen in the first energy spectrum (dashed line). This follows from the sum of its emitted velocity plus the extra "kick" it gets from the fragment's velocity. Conversely, SST 2 is positioned so that it receives ^{4}He preferentially from the undetected fragment. These particles will have larger lab velocities and energies (dashed-dot line) than those from the detected fragment (dashed line), as this fragment is moving in the opposite direction from the ^{4}He that strikes SST 2. Prefission ^{4}He emission (light solid line) will have the highest average lab energies in the most forward directions, that is, in SST's 3 and 4, as shown by the large lab velocities indicated in the out-of-plane vector diagram.

D. ^{1}H and ^{4}He multiplicities for FF/DIR

The kinematic shifts discussed in the previous section allow us to identify each source's individual contribution to the observed particle spectrum. We do this by normalizing the simulated spectra to the experimental data so that their sum (heavy solid line shown in each of the spectra in Figs. 4 and 5) matches the experimental spectrum as closely as possible. We are then able to calculate upper limits for the differential cross section for ^{4}He from each source. Equation (4.1) is then used to obtain the particle multiplicity from each source. (See Refs. [1] and [12] for further discussion.) Multiplicities for the combined FF/DIR reaction class are listed in Table II. Note that multiplicities are listed for both fragment emission (FE) and composite emission (CE) in accordance with the source identification discussed above. Multiplicities for FE are for the combined fragment emission so that these average multiplicities are the total per fission event.

Multiplicities associated with the FF/DIR reaction class will be discussed below after we obtain particle multiplicities associated with the ER's. We present them now to illustrate the technique of their derivation and to point out the magnitude of the CE multiplicities listed in Table II for the FF/DIR class. Approximately one third to one half of the particle cross sections associated with these nuclear systems of high spin (the FF/DIR class) are emitted by the composite system prior to separation into two fragments. We will return to this interesting point later. For now, let us look at the ^{1}H and ^{4}He multiplicities associated with ER's.

V. PARTICLE CROSS SECTIONS AND MULTIPLICITIES FOR ER's

An indirect method is used to assign the ^{1}H or ^{4}He multiplicities for the ER's because ER-particle coincidences were not measured in these experiments. We obtain ^{1}H or ^{4}He particle multiplicities associated with the ER reaction class by use of Eq. (4.1). The cross section $\sigma_s^p(\mathrm{ER})$ is derived (by difference) from the singles proton cross section (σ_s^p) and the combined FF/DIR particle contributions as follows:

$$\sigma_s^p(ER) = \sigma_s^p - \sigma(\mathrm{FF/DIR})\langle m^p(\mathrm{CE})\rangle - \sigma(\mathrm{FF/DIR})\langle m^p(\mathrm{FE})\rangle \,. \quad (5.1)$$

TABLE II. Light-charged particle multiplicities.

Particle	Total	^{1}H and ^{4}He multiplicities ER	FF/DIR (FE)	FF/DIR (CE)
^{1}H	1.22 ±0.25	1.63 ±0.39	0.643 ±0.045	0.301 ±0.021
^{4}He	0.96 ±0.19	1.62 ±0.33	0.255 ± 0.018	0.277 ±0.019

		IMF light charged particle multiplicities CE[a]	IMFE[a]	HFE[a]
$3 \le Z \le 10$	^{4}He	0.4	0.06	0.2
	^{1}H	0.4	0.05	1.1
$11 \le Z \le 18$	^{4}He	0.2	0.3	0.2
	^{1}H	0.06	0.2	0.5

[a]Uncertainties are estimated as ≈25%.

The ER-particle multiplicity for particle type x (e.g., p for proton) is then

$$\langle m^p(\mathrm{ER})\rangle = \frac{\sigma_s^p(\mathrm{ER})}{\sigma_s(\mathrm{ER})} \,. \tag{5.2}$$

Other reaction classes are expected to make a negligible contribution to the inclusive cross section [1] and are not included in these calculations. The values of $\sigma(\mathrm{ER})$ [i.e., $\sigma_s(\mathrm{ER})$, $\sigma_s^p(\mathrm{ER})$, and $\sigma_s^\alpha(\mathrm{ER})$] are listed in Table I; the corresponding ER multiplicities are given in Table II.

A. Particle-particle coincidence cross sections associated with ER's

We may also obtain the double coincidence (dc) angle-integrated particle cross sections σ_{dc}^{pp}, $\sigma_{dc}^{\alpha\alpha}$, and $\sigma_{dc}^{p\alpha}$ from the particle-particle coincidence cross sections. These total double-coincidence cross sections include contributions from the fragments and the prescission nucleus. It is therefore necessary to estimate their separate contributions in order to derive the double-coincidence cross sections associated with the ER's. In Ref. [2] a method is described for deriving fragment-particle-particle coincidence cross sections from CE and FE multiplicities. Following this method, fragment-particle-particle cross sections have been estimated for the 640 MeV ^{86}Kr + ^{63}Cu reaction from the FF/DIR multiplicities listed in Table I. The particle-particle cross sections in association with the ER's may then be obtained from the following simple relation (illustrated for ^{1}H-^{1}H coincidences):

$$\sigma_{dc}^{pp}(\mathrm{ER}) \;=\; \sigma_{dc}^{pp} - \sigma_{dc}^{pp}(\mathrm{FF/DIR}) \,, \tag{5.3}$$

where the final term represents the combined CE and FE contributions arising from FF/DIR processes. Similar equations may be written for ^{1}H–^{4}He and ^{4}He–^{4}He coincidences. The observed total double-coincidence cross sections, along with the derived values for the contribution from ER's, are listed in Table I. For the example shown in Eq. (5.3), $\sigma_{dc}^{pp}(\mathrm{FF/DIR})$ is estimated as 326 mb, a small quantity relative to the total σ_{dc}^{pp} cross section of 1220 mb. We conclude that decay chains with two or more light-charged particles are mainly produced in the most central collisions between target and projectile.

VI. MECHANISTIC IMPLICATIONS OF ER AND FF/DIR PARTICLE MULTIPLICITIES AND CROSS SECTIONS

Let us summarize what has been noted thus far. Three observations may be made based on the information in Tables I and II: (1) CE multiplicities for the ER class are substantially larger than those for the FF/DIR class; (2) Decay chains involving the evaporative emission of at least two light-charged particles come primarily from emitters that decay to ER's; and (3) CE multiplicities for FF/DIR are quite significant (even though they are less than those for the ER's). We now discuss the qualitative significance of these three observations.

(1) The small (relative to ER) CE multiplicities for the FF/DIR class probably reflect the competition from fission. We may therefore conclude that the magnitude of these multiplicities is driven in part by the dynamics of the fission process, viz., the relative timescales for evaporation versus fission.

(2) The data in Table I show that the total double-coincidence cross sections listed are only slightly larger than the subset associated with the ER reaction class. This indicates that nuclear reactions that produce decay chains with at least two light-charged particles mainly result from these ER's, i.e., the more central collisions between target and projectile. Only small double-coincidence coincidence cross sections have been estimated or observed for the FF/DIR reaction class. The large cross sections associated with the ER's are consistent with the view that these emitters have relatively low rotational energies and relatively high temperatures.

(3) Significant CE multiplicities associated with the FF/DIR reaction class have been observed before [1]; they are surprising because much of the spin zone is greater than the predicted spin value at which the fission barrier vanishes [13]. This observation suggests a rather long time during which even the so-called "fast fission" process transpires, long enough for particle evaporation to compete with scission. These CE multiplicities are hard to reconcile with a view of fission that occurs extremely rapidly. This conclusion is consistent with experimental prescission neutron multiplicities that are also greater than those predicted by the statistical model [14,15]. It would seem that, in addition to the availability of phase space, dynamical effects are also involved in driving these fissionlike and/or evaporationlike processes.

VII. IMF PARTICLE MULTIPLICITIES AND PRIMARY MASSES

The emission of ^{1}H and ^{4}He has also been studied in coincidence with two broad IMF groups for the reaction 640 MeV ^{86}Kr + ^{63}Cu, Group I is for $3 \leq Z_{\mathrm{IMF}} \leq 10$ and Group II is for $11 \leq Z_{\mathrm{IMF}} \leq 18$. These groups, in place of individual fragments, were chosen to ensure sufficient statistics for comparison to statistical-model reaction simulations.

We have previously reported [5] that $\approx$90% or more of the IMF yields are produced by asymmetric binary breakup for this reaction. The code GANES was therefore employed to generate lab energy spectra for each emission source. These sources, analogous to those discussed for symmetric fission, are (1) composite systems prior to scission (CE), (2) the detected IMF (IMFE), and (3) the undetected heavy fragment (HFE) associated with the specific IMF. The observed energy spectra, as well as the simulated spectra and their sums for both IMF trigger groups, are shown in Figs. 6–9. Multiplicities have been derived in the same manner as discussed above for symmetric fission, and the results are summarized in Table II.

The method of extracting the light-charged particle

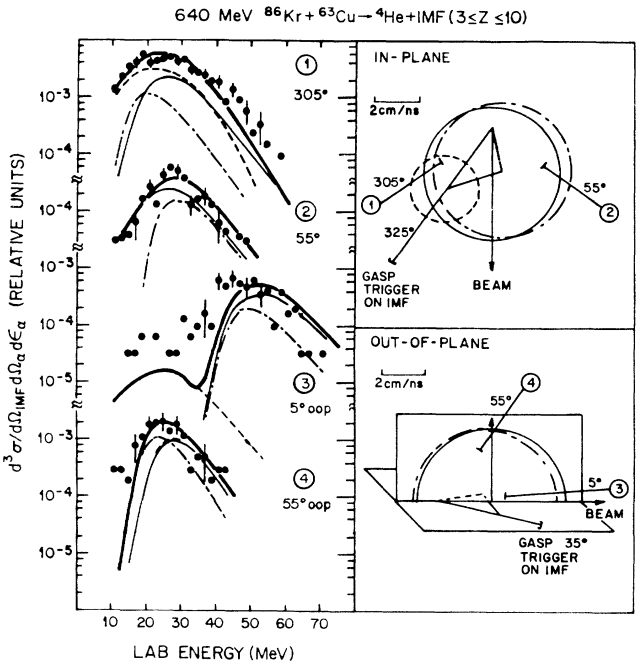

FIG. 6. Same as Fig. 4 but for trigger fragments of $3 \leq Z \leq 10$.

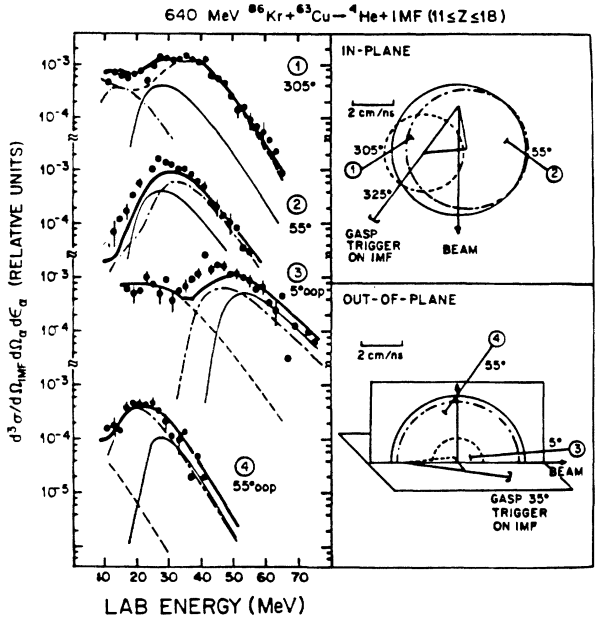

FIG. 8. Same as Fig. 4 but for trigger fragments of $11 \leq Z \leq 18$.

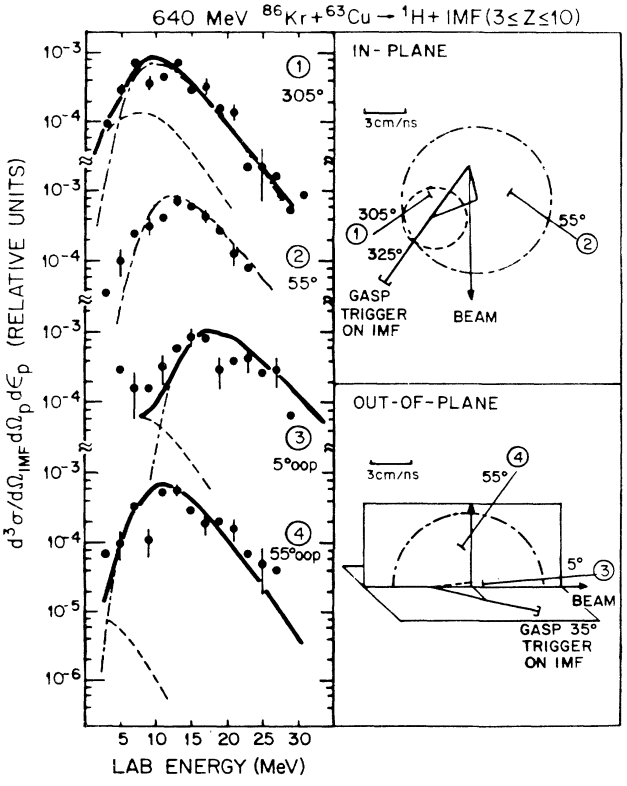

FIG. 7. Same as Fig. 6 but for ^{1}H emission. Emission from the composite system is not included. The small kinematic shift in ^{1}H energy between composite and heavy fragment ^{1}H emission precluded a clear separation of sources.

multiplicities for each source from the energy spectra has already been discussed in Sec. VI. The same technique applies for asymmetric fission. We note from Figs. 6–9, however, that the recoil velocity of the undetected heavy fragment is significantly less for asymmetric fission. This reduces our sensitivity to make a clear separation of emission sources between the composite nucleus and heavy fragment because the kinematic shifts in particle ener-

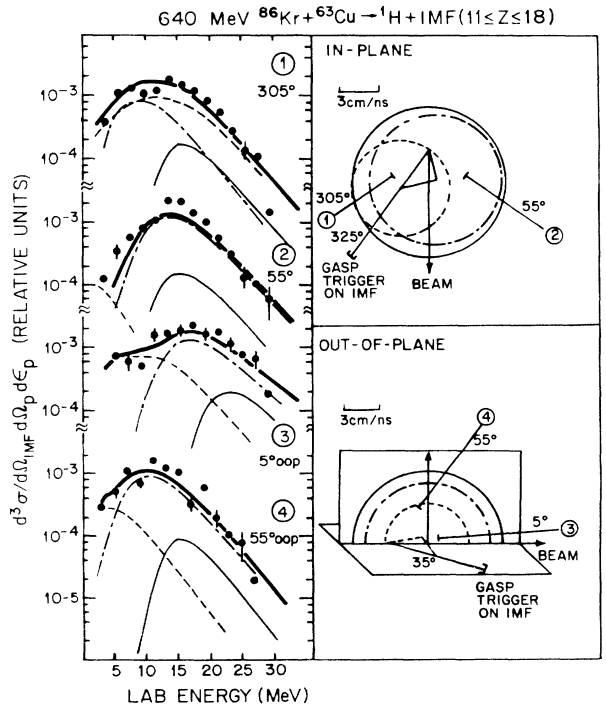

FIG. 9. Same as Fig. 8 but for ^{1}H emission.

gies from these sources are so small. This is particularly true for very asymmetric fission (Group I), as shown in Figs. 6 and 7. For the case of ^{1}H emission in association with IMF's of $3 \leq Z \leq 10$ (Fig. 7), emission from the composite system could indeed not be distinguished from the heavy fragment. This results from the combined effects of a small recoil velocity for the heavy fragment and a large velocity for such a light particle as ^{1}H. We make the simplifying assumption that ^{1}H emission from the composite nucleus prior to scission is the same as ^{4}He emission, as listed in Table II under the column headed "CE." This is based on the observation for the ER and FF/DIR classes. Results appear to be different for the IMF group II, but those multiplicities are small and thus more subject to error.

A. Primary masses of the IMF's

The ^{1}H and ^{4}He multiplicities for the IMF's that are given in Table II allow us to estimate the average primary charge and mass of each IMF along with the associated total kinetic energy (TKE). These particle multiplicities indicate that the IMF's are born with some excitation energy and, hence, evaporate particles *en route* to the detector. Thus the detected charge and mass are, on average, less than the primary charge and mass. The procedure for calculating the detected and primary average masses is discussed in Appendix A, and results are summarized in Table III.

We first note from Table III that the detected charge Z is integral, but not so for the primary charge, nor for any of the masses A. For any given particle, the values of A and Z are, of course, integral. Nonintegral values simply mean that an average has been taken over an ensemble of fragments that vary in their individual masses and charges. For example, for a detected charge of $Z = 11$, the average primary charge and mass are estimated to be 11.69 and 26.70, respectively. This means, on average, 0.69 charge units are evaporated from an ensemble of particles with an average mass of 26.70 amu. (See Appendix A.) This ensemble decays to another ensemble with a detected charge of $Z = 11$ and an average mass of 25.19 u. The detected charge is integral because we detect and separate the charges of the various IMF's, not their masses. In other words, we have good Z resolution but no direct mass determination.

Note that the multiplicities for Group I in Table II indicate that, on average, 0.17 charge units are evaporated ($0.0585 \times 2 + 0.0487 = 0.166$). This value is taken to be constant within this group because the light-charged particle multiplicities were averaged over this group. For Group II, the average charge evaporated is 0.69 charge units. This is interpreted as resulting from an increase in the share of excitation energy for this group of heavier IMF's. Note also that the differences between primary masses and observed masses increase with increasing Z. The greater the amount of excitation energy partitioned to a fragment, the greater the number of evaporated particles it emits.

The values of the TKE's in Table III differ slightly from those in Ref. [5]. There, a comparison was made between the experimental TKE's and theoretical saddle and scission point calculations. Similar data and comparisons have also been published in [19] (for ^{98}Mo + ^{51}V). Both here and in Refs. [5] and [19] the TKEs were calculated by the method outlined in Appendix A. The values listed in Table III are from our second experiment (as discussed in Sec. II), and are given here because of their improved statistical significance. The conclusion that the IMF's are produced primarily by asymmetric binary fission was drawn in Refs. [5,19]; these small differences would not alter that conclusion.

VIII. SUMMARY AND CONCLUSIONS

From the inclusive and coincidence measurements that are reported in this paper, we come to the following findings and conclusions:

(1) The invariant cross sections for inclusive ^{4}He emission, the ^{4}He angular distribution, and the c.m. energy

TABLE III. IMF masses (A), charges (Z), and total kinetic energies (TKE) from 640 MeV ^{86}Kr + ^{63}Cu.

Detected		Primary		Scissioner			
Z	A	Z	A	Z	A	$E_{\text{c.m.}}$ (MeV)[a]	TKE (MeV)[b]
4	8.18	4.17	9.50			32.5	40.4 ±4.4
5	10.46	5.17	11.77			34.7	42.6 ±4.7
6	13.17	6.17	14.05			37.8	44.7 ±5.0
7	15.17	7.17	16.33	63.80	145.3	42.9	52.0 ±5.3
8	17.53	8.17	18.61			46.8	57.0 ±4.1
9	19.94	9.17	20.88			51.2	62.5 ±3.6
10	22.20	10.17	23.16			53.1	65.9 ±3.0
11	25.19	11.69	26.70			55.1	71.4 ±3.1
12	27.08	12.69	28.98			58.0	77.2 ±2.6
13	29.26	13.69	31.26	64.61	147.54	59.6	80.7 ±3.5
14	31.22	14.69	33.55			59.2	82.4 ± 2.1

[a]Listed values are derived using the detected IMF masses as described in the appendix.
[b]Listed values are calculated with the primary IMF masses.

spectra for ^{1,2,3}H and ^{4}He are consistent with evaporation as the dominant mechanism for their production.

(2) ^{1}H and ^{4}He evaporative emissions from the FF/DIR reaction classes are significant. However, the largest fractions of the inclusive particle cross sections are associated with the ER's [^{1}H (53%) and ^{4}He (67%)]. For the particle-particle coincidence cross sections, substantially greater fractions are associated with the ER's [^{1}H-^{1}H (87%), ^{4}He-^{4}He (91%), and ^{1}H-^{4}He (65%)].

(3) The IMF's are born with a significant amount of excitation energy, as indicated by their post-scission ^{1}H and ^{4}He multiplicities.

(4) The IMF particle multiplicities allow one to derive the average masses of the primary fragments. Estimates of both the primary and final masses are required in order to derive the IMF total kinetic energies, as detailed in Appendix A and listed in Table III.

ACKNOWLEDGMENTS

The GASP detectors discussed in Sec. II were designed and built at Lawrence Berkeley Laboratory with the guidance of G. Wozniak and L. Sobotka. The staff of the Lawrence Berkeley Laboratory SuperHilac is gratefully acknowledged. We thank W. Parker for many helpful discussions. This work was supported by the Division of Nuclear Physics, Office of High Energy and Nuclear Physics, U.S. Department of Energy.

APPENDIX: DERIVED IMF MASSES, CHARGES, AND TOTAL KINETIC ENERGIES

The IMF multiplicities listed in Table II allow us to estimate the average primary charge and mass of each IMF. These multiplicities indicate that the IMF's are born with substantial excitation energy and hence evaporate particles. Thus the detected charge and mass is smaller than the primary charge and mass. Both primary and detected masses are required to correct the detected energies in order to obtain the primary total kinetic energy (TKE) released.

The need for both masses becomes clear when we write the equation for the TKE derived simply from momentum conservation,

$$\mathrm{TKE} = E_{\mathrm{c.m.}} \left\{ 1 + \frac{A_{\mathrm{IMF}}}{A_{\mathrm{HF}}} \right\} , \tag{A1}$$

$$A_{\mathrm{HF}} = A_{\mathrm{sciss}} - A_{\mathrm{IMF}} , \tag{A2}$$

where $E_{\mathrm{c.m.}}$ is the center-of-mass energy of the primary IMF, A_{IMF} (A_{HF}) is the mass of the IMF (heavy fragment), and A_{sciss} is the mass of the fissioning nucleus (i.e., the scissioner). The sum within braces in Eq. (A1) includes the recoil energy of the heavy fragment so that the TKE is the sum of the IMF and heavy-fragment kinetic energies.

The detected energy of the IMF ($E^{\mathrm{obs}}_{\mathrm{c.m.,IMF}}$) arises from a mass that is slightly smaller than that of the primary IMF. Therefore the kinetic energy of the primary IMF is slightly larger:

$$E_{\mathrm{c.m.,IMF}} = E^{\mathrm{obs}}_{\mathrm{c.m.,IMF}} \left\{ \frac{A_{\mathrm{IMF}}}{A^{\mathrm{obs}}_{\mathrm{IMF}}} \right\} , \tag{A3}$$

where $A^{\mathrm{obs}}_{\mathrm{IMF}}$ is the mass of the IMF as it enters the detector, and A_{IMF} is the primary IMF mass. We neglect any change in average velocity due to particle emission from the IMF. Thus both masses are required to compute primary TKE values from Eq. (A1). The estimation of these masses is a multistep operation.

The first step is to calculate the mass and charge of the composite nucleus prior to scission. The mass of the scissioner is estimated from the light particle multiplicities for composite emission (CE). A statistical-model calculation (CASCADE [16]) was used to obtain the ratio of neutrons to alpha particles ($0 < J < 72\hbar$), as neutrons were not detected in the experiments discussed here. This ratio is then used to obtain the prescission neutron multiplicity from the experimentally derived ^{4}He multiplicity.

By way of illustration, assume the IMF has a detected charge ($Z^{\mathrm{obs}}_{\mathrm{IMF}}$) of 14. Multiplicities for composite emission of ^{1}H and ^{4}He are 0.0603 and 0.167, respectively, as indicated in Table II. This means that, on average, for IMF's of $11 \leq Z_{\mathrm{IMF}} \leq 18$ the charge of the scissioner is

$$Z_{\mathrm{sciss}} = 65 - 2(0.167) - 1(0.0603) = 64.61 , \tag{A4}$$

where 65 is the initial charge of the ^{149}Tb composite nucleus. A similar procedure is followed to obtain its mass, except that the masses of the particles are used instead of their charges

$$\begin{aligned} A_{\mathrm{sciss}} &= 149 - 4(0.167) - 1(0.0603) - 1(0.732) \\ &= 147.54 \text{ u} , \end{aligned} \tag{A5}$$

where the quantity 0.732 is the prefission neutron multiplicity from the calculated ratio of n to ^{4}He evaporation.

The assumption is made in the next step of the calculation that the mass-to-charge ratio of the scissioner is the same as that for the primary fragments. In the case of the IMF group to which $Z^{\mathrm{obs}}_{\mathrm{IMF}} = 14$ belongs, this value is 2.28 (i.e., 147.54 / 64.61). The implicit assumption is that the projectile and target have fused, lost their individual identities, and have completely mixed their nucleons so that this charge-to-mass ratio remains constant.

In order to compute the charge of the primary IMF, one starts with the detected charge (integer) of the IMF ($Z^{\mathrm{obs}}_{\mathrm{IMF}}$). The ^{1}H and ^{4}He multiplicities for IMF emission (listed under the column "IMFE" in Table II) are then used to obtain the average primary charge of the IMF in the same manner as Z_{sciss} was obtained. Thus

$$Z_{\mathrm{IMF}} = Z^{\mathrm{obs}}_{\mathrm{IMF}} + 2\langle m_\alpha \rangle^{\mathrm{IMFE}} + 1\langle m_p \rangle^{\mathrm{IMFE}} , \tag{A6}$$

where, for $Z^{\mathrm{obs}}_{\mathrm{IMF}} = 14$, the primary charge is

$$Z_{\mathrm{IMF}} = 14 + 2(0.252) + 1(0.186) = 14.69 . \tag{A7}$$

Multiplying Z_{IMF} by the mass-to-charge ratio of the scissioner discussed above,

$$A_{\rm IMF} = Z_{\rm IMF}\left\{\frac{A_{\rm sciss}}{Z_{\rm sciss}}\right\} \tag{A8}$$

gives the primary mass of the IMF, such that, in the case of our example,

$$A_{\rm IMF} = 14.69 \times 2.28 = 33.50 \text{ u} . \tag{A9}$$

We now need to estimate $A^{\rm obs}_{\rm IMF}$. Because we already know ^{1}H and ^{4}He multiplicities for IMF emission, we also know how much mass was removed by charged particles from the primary IMF in transit to the detector. To calculate $A^{\rm obs}_{\rm IMF}$, we also need to know the neutron multiplicities for each IMF, where

$$A^{\rm obs}_{\rm IMF} = A_{\rm IMF} - 4\langle m_\alpha\rangle^{\rm IMFE} - \langle m_p\rangle^{\rm IMFE} - \langle m_n\rangle^{\rm IMFE} . \tag{A10}$$

We may estimate $\langle m_n\rangle^{\rm IMFE}$ by assuming all the excitation energy of the primary mass is depleted by particle emission. In general, the average excitation energy removed by one particle is

$$E^{*\rm rem}_{n,p,\alpha} = E^{\rm sep}_{n,p,\alpha} + \epsilon_{n,p,\alpha} , \tag{A11}$$

where $E^{\rm sep}_{n,p,\alpha}$ is the separation energy of the neutron (n), proton (p), or alpha (α), and $\epsilon_{n,p,\alpha}$ is the average kinetic energy of the respective particle.

In order to derive the excitation energy of the primary IMF, we need to compute the initial excitation energy of the scissioner, as it is this excitation energy that is partitioned between the primary fragments. We may therefore write

$$E^*_{\rm sciss} = E^*_0 - \langle m_\alpha\rangle^{\rm CE}E^{*\rm rem}_\alpha - \langle m_p\rangle^{\rm CE}E^{*\rm rem}_p - \langle m_n\rangle^{\rm CE}E^{*\rm rem}_n \tag{A12}$$

and

$$E^*_{\rm IMF} = E^*_{\rm sciss}\left\{\frac{A_{\rm IMF}}{A_{\rm sciss}}\right\} , \tag{A13}$$

where the superscript CE denotes that these are particle multiplicities for composite emission. For the case of $Z^{\rm obs} = 14$,

$$E^*_{\rm IMF} = 142.52 \text{ MeV} \times 0.227 = 32.36 \text{ MeV} . \tag{A14}$$

The excitation energy of the primary IMF, however, is partitioned between thermal excitation and rotational energy. It is the thermal excitation energy that drives the particle multiplicities and thus determines the value of $\langle m_n\rangle^{\rm IMFE}$ used in Eq. (A10). We therefore need to subtract a rotational energy from $E^*_{\rm IMF}$. The rotational energy of the IMF may be obtained by partitioning the root-mean-square spin of the scissioner, according to the rigid rotor hypothesis

$$J^{\rm rms}_{\rm IMF} = J^{\rm rms}_{\rm sciss}\frac{\Im_{\rm IMF}}{\Im_{\rm IMF} + \Im_{\rm HF} + \mu R^2} , \tag{A15}$$

where $\Im_{\rm IMF}$ and $\Im_{\rm HF}$ are the spherical moments of inertia of the IMF and heavy fragment (HF). The radial distance R between the centers of the IMF and HF has been taken as that for touching spheres, and μ is the reduced mass of the system. The value of $J^{\rm rms}_{\rm sciss}$ is derived from the ER spin zone of 0–72$\hbar$ for the 640 MeV ^{86}Kr + ^{63}Cu reaction [12]. Knowledge of $J^{\rm rms}_{\rm IMF}$ thus allows us to estimate the rotational energy of the IMF

$$E_{\rm rot,IMF} = \frac{(J^{\rm rms}_{\rm IMF})^2\hbar^2}{2\Im_{\rm IMF}} . \tag{A16}$$

We are now in a position to calculate $\langle m_n\rangle^{\rm IMFE}$ in Eq. (A10) and thus $A^{\rm obs}_{\rm IMF}$. The essential equation is

$$\langle m_n\rangle^{\rm IMFE} = \frac{E^*_{\rm IMF} - E_{\rm rot,IMF} - \langle m_\alpha\rangle^{\rm IMFE}E^{*\rm rem}_\alpha - \langle m_p\rangle^{\rm IMFE}E^{*\rm rem}_p - E_\gamma}{E^{*\rm rem}_n} , \tag{A17}$$

where E_γ equals half the neutron binding energy if an additional neutron were evaporated by the IMF. This approximates the excitation energy removed by γ rays, as the probability for the emission of an additional neutron is very low when the excitation energy is close to the neutron binding energy.

With $\langle m_n\rangle^{\rm IMFE}$ now evaluated, Eq. (A10) may be used to obtain $A^{\rm obs}_{\rm IMF}$. Use of both $A^{\rm obs}_{\rm IMF}$ and $A_{\rm IMF}$ now allows the calculation of $E_{\rm c.m.,IMF}$ from Eq. (A3) and subsequently the TKE from Eq. (A1). This is the desired result. Table III lists the detected and primary IMF masses and charges, those of the scissioners, the observed $E_{\rm c.m.}$, and the values of the primary TKE.

[1] R. Lacey, N. N. Ajitanand, J. M. Alexander, D. M. de Castro Rizzo, G. F. Peaslee, L. C. Vaz, M. Kaplan, M. Kildir, G. La Rana, D. J. Moses, W. E. Parker, D. Logan, M. S. Zisman, P. DeYoung, and L. Kowalski, Phys. Rev. C **37**, 2561 (1988).

[2] R. Lacey, N. N. Ajitanand, J. M. Alexander, D. M. de Castro Rizzo, G. F. Peaslee, L. C. Vaz, M. Kaplan, M. Kildir, G. La Rana, D. J. Moses, W. E. Parker, D. Logan, M. S. Zisman, P. DeYoung, and L. Kowalski, Phys. Rev. C **37**, 2540 (1988).

[3] J. Boger, John M. Alexander, R. Lacey, and A. Narayanan, accompanying paper, Phys. Rev. C **49**, 1587 (1994).

[4] N. N. Ajitanand, R. Lacey, G. F. Peaslee, E. Duek, and

J. M. Alexander, Nucl. Instrum. Methods, Phys. Res. A **243,** 111 (1986).

[5] J. Boger, S. Kox, G. Auger, J. M. Alexander, A. Narayanan, M. A. McMahan, D. J. Moses, M. Kaplan, and G. P. Gilfoyle, Phys. Rev. C **41**, R801 (1990).

[6] D. J. Moses, Ph.D. dissertation, Dept. of Chemistry, Carnegie-Mellon University (1986).

[7] D. J. Moses, M. Kaplan, J. M. Alexander, D. Logan, M. Kilder, L. C. Vaz, N. N. Ajitanand, E. Duek, and M. S. Zisman, Z. Phys. A **320,** 229 (1985).

[8] V. E. Viola, K. Kwiatkowski, and M. Walker, Phys. Rev. C **31,** 1550 (1985).

[9] M. Kildir, D. Logan, D. O. Eriksen, D. J. Moses, M. Kaplan, E. Duek, L. C. Vaz, N. N. Ajitanand, J. M. Alexander, and M. S. Zisman, Z. Phys. A **317,** 291 (1984).

[10] E. Duek, N. N. Ajitanand, J. M. Alexander, D. Logan, M. Kildir, L. Kowalski, L. C. Vaz, D. Guerreau, M. S. Zisman, and M. Kaplan, Phys. Lett. **131B,** 297 (1983).

[11] D. J. Moses, M. Kaplan, M. Kilder, D. R. G. Logan, G. LaRana, W. E. Parker, R. Lacey, G. F. Peaslee, J. M. Alexander, N. N. Ajitanand, L. C. Vaz, and M. S. Zisman, Nucl. Phys. **A465,** 339 (1987).

[12] J. Boger, Ph.D. dissertation, Dept. of Chemistry, State University of New York at Stony Brook (1992).

[13] S. Cohen, F. Plasil, W. J. Swiatecki, Ann. Phys. (NY) **82,** 557 (1974).

[14] A. Gavron, A. Gayer, J. Boissevain, H. C. Britt, T.C. Awes, J. R. Beene, B. Cheynis, D. Drain, R. L. Ferguson, F. E. Obenshain, F. Plasil, G. R. Young, G. A. Petitt, and C. Butler, Phys. Rev. C **35,** 579 (1987).

[15] J. B. Natowitz, M. Gonin, K. Hagel, R. Wada, S. Shlomo, X. Bin, M. Gui, Y. Lou, D. Utley, T. Botting, R. K. Choudhury, L. Cooke, B. Hurst, D. O'Kelly, R. P. Schmitt, W. Turmel, H. Utsunomiya, G. Nebbia, D. Fabris, J. A. Ruiz, G. Nardelli, M. Poggi, R. Zanon, G. Viesti, R. H. Burch, F. Gramegna, G. Prete, D. Drain, B. Chambon, B. Cheynis, D. Guinet, X. C. Hu, A. Demeyer, C. Pasteur, A. Giorni, A. Lleres, P. Stassi, B. Viano, A. Menchaca Rocha, M. E. Brandan, and P. Gonthier, Nucl. Phys. **A538,** 263c (1992).

[16] E. Puehlhofer, Nucl. Phys. **A213,** 267 (1977).

[17] F. Plasil, R. L. Ferguson, H. C. Britt, B. H. Erkkila, P. D. Goldstone, R. J. Stokes, and H. H. Gutbrod, Phys. Rev. C **18,** 2603 (1978).

[18] H. C. Britt, B. H. Erkkila, R. H. Stokes, H. H. Gutbrod, F. Plasil, R. L. Ferguson, and M. Blann, Phys. Rev. C **13,** 1483 (1976).

[19] N. Carjan and M. Kaplan, Phys. Rev. C **45,** 2185 (1992).